A Rocket Investigation of Mesospheric Eddy Diffusion Effects on Airglow and Oxygen Chemistry

Final Report
NASA Grant NAG5-5046
30 November 2001

James C. Ulwick
Stewart Radiance Laboratory/Space Dynamics Laboratory
Utah State University Research Foundation
139 The Great Road
Bedford, MA 01730
Telephone: (617) 275-8273
Fax: (617) 271-0535

Table of Contents

List of Figures

Abstract

A Terrier Orion rocket was launched at 0750 Z on 02/25/98 about seven minutes after the Clemson University chemical release rocket. Measurements made of the electron density by a dc probe calibrated by a capacitance probe showed several layers of electron density on a rocket ascent in the altitude range from 90 to 110 km. Rocket descent results showed several but not all of the ascent structure. From power spectral analysis of the measured electron densities, turbulent parameters are derived. Measurements were made on rocket ascent and descent by an infrared radiometer of the OH Meinel (3-1) band and O_2 singlet delta emissions. Profiles of the emissions are presented and discussed. On both rocket ascent and descent an enhancement of the OH emission monitored by the OH radiometer was observed above 90 km. The glow was not detected by the O_2 radiometer and was significantly reduced on rocket descent. Using these data and a mechanistic analysis, a profile proportional to atomic oxygen is obtained. This profile is compared to one from the ATOX probe on the rocket. A one-dimensional (1-D) photochemical model that solves the time-dependent continuity equations is used with the rocket data to investigate the odd-oxygen concentration in the near equatorial mesosphere.

1.0 Introduction

The Space Dynamics Laboratory (SDL) of the Utah State University Research Foundation participated in the NASA sponsored Coqui Dos Campaign in Puerto Rico in February of 1998. The overall objective of the Coqui Dos Campaign was to measure the properties of turbulent layers, ionization layers, and sudden atom layers in the mesosphere and lower thermosphere. Instrumentation on the SDL Terrier Orion rocket measured the vertical structure of OH, O, O_2* emission profiles along with the small-scale structure in the electron density profile. All launches were carried out from the temporary launch facility which was established and operated by Goddard Wallops Flight Facility personnel at Tortuguero on the northwest coast of Puerto Rico. All rockets were launched towards the northwest and impacted into the ocean. The SDL rocket, which was nicknamed Eddy, was launched at 0750 Z (0350 LT) on 25 February 1998 and reached an altitude of 129 km. Seven minutes after it was launched, a Clemson University chemical release rocket was launched for the measurement of eddy and molecular diffusivity from the rate of expansion of the trails obtained from photographic data from three ground sites. Ground-based incoherent scatter radar and sodium lidar measurements at the nearby Arecibo Observatory were critical in determining the launch conditions.

In this report, the results of the SDL rocket flight are presented. Measurements made of the electron density by a dc probe calibrated by a capacitance probe showed several layers of electron density on rocket ascent in the altitude range from 90 to 110 km. Rocket descent results showed several but not all of the ascent structure. From power spectral analysis of the measured electron densities, turbulent parameters are derived. Measurements were made on rocket ascent and descent by an infrared radiometer of the OH Meinel (3-1) band and O_2 singlet delta emissions. Profiles of the emissions are presented and discussed. On both rocket ascent and descent, an enhancement of the OH emission monitored by the OH radiometer was observed above 90 km. The glow was not detected by the O2 radiometer and was significantly reduced on rocket descent. Using these data and a mechanistic analysis, a profile proportional to atomic oxygen is obtained. This profile is compared to one from the ATOX probe on the rocket. A one-dimensional (1-D) photochemical model that solves the time-dependent continuity equations is used with the rocket data to investigate the odd-oxygen concentrations in the near equatorial mesosphere.

2.0 Instrumentation

Measurements of OH, O_3, O_2* and O were to be accomplished using both photometric and in-situ, resonance-fluorescence methods. Additionally, we would measure the structure and concentration of electrons as a function of height using an in-situ DC/Capacitance probe (Ulwick et al., 1988). The rocket payload was for a Terrier-Orion rocket and utilized flight-proven, modular instrumentation designed and developed at USU. The payload, which was 17.26" in diameter, is approximately 32.7" long and weighs approximately 114 pounds. Figure 1 is a sketch of the payload after nosecone ejection.

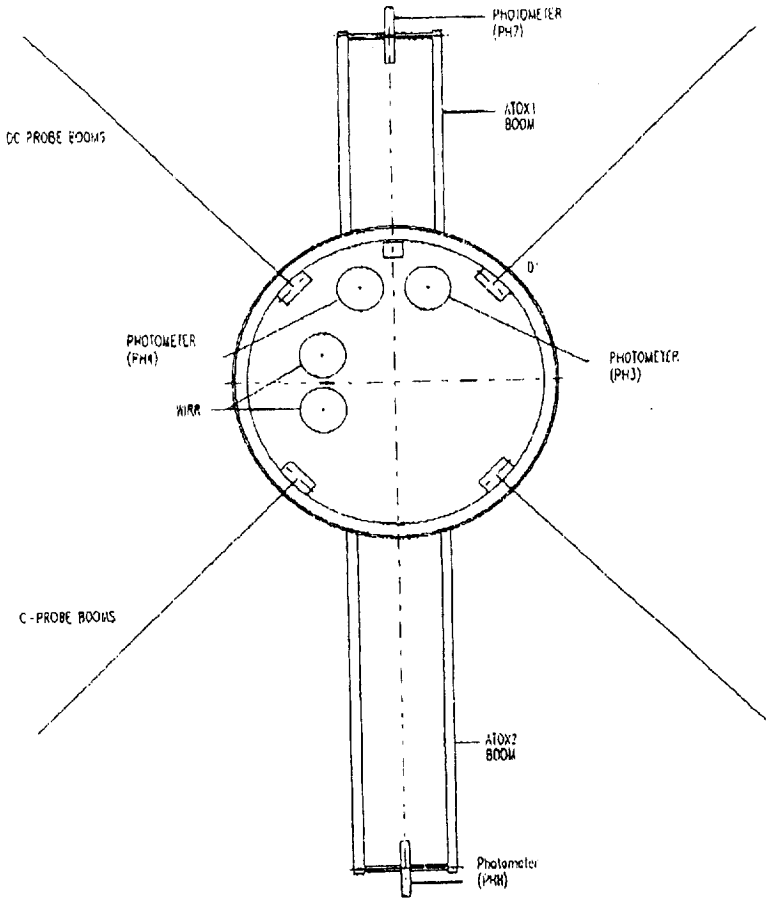

Figure 1 Sketch of payload and the probes location

2.1 DC and Capacitance Probe (DC-Probe and C-Probe)

We used a combination of an RF capacitance probe and a fixed potential Langmuir Probe (DC Probe) to measure electron density and its structure. This combination has proven successful in providing high spatial resolution for irregularities and accurate absolute values (Ulwick et al., 1988). The Capacitance probe measures the antenna's free space capacitance and impedance extending into the plasma. Electron density is deducted from changes in capacitance impedance as the rocket flies through the plasma. The DC probe measures the current to a small electrode held at a fixed potential a few volts. The collected current is converted to a 16-bit digital number and is transmitted to the ground. While this technique only provides a relative measure of density, it can be normalized to absolute value provided by the C-Probe. This DC probe gives high spatial resolution of density changes (~.3 m).

Each of the probes were mounted at the front of the payload, at the separation plane of the nose-cone. The probes will consist of four, fold-down wire antennae, ~1/16" diameter that extend up into the clamshell nose-cone for launch. As the nose-cone deploys, these antennae fold down into place 90° to the rocket axis. In the deployed position, these antennae are rotated 45° with respect to the ATOX boom systems. The DC probe consists of one pair of booms while the C-Probe is the other orthogonal pair. The DC probe has one signal channel, and the C-Probe has two.

2.2 Atomic Oxygen Resonance Fluorescence

Each instrument (two systems) consists of an RF discharge lamp [ATOX1 and ATOX2], a 130-nm pulse counting photometer [PH5(ATOX1) and PH6(ATOX2)], and a photometer absorption measurement [PH7(ATOX1) and PH8(ATOX2)]. The lamp is typically modulated at 200 Hz to provide a high vertical resolution measurement of the background and fluorescence signals from which the atomic oxygen is derived. The photometers (PH5 and PH6) have an additional current output which gives them a full dynamic range of 7.5 decades. Each photo-diode measurement is deployed on booms opposite each other to provide an absolute atomic oxygen value free of shock and vehicle outgassing effects. Recently, Utah State University, Stockholm University and Aerodyne Laboratories have jointly calibrated the lamps in a flowing afterglow system.

Each ATOX system was mounted opposite each other in the rear of the instrument section, and viewed horizontally (45° to the rocket axis, 180° between each lamp/boom system). Each ATOX system required an ejectable door (total 2), and each deployed lightweight boom system (total 2) through the door. Each lamp (ATOX1 and ATOX 2) required a monitor of its UV output (1/on cycle, 1/off cycle), and a monitor of the getter temperature. Each photometer (PH5 and PH6) required two signal channels and one high-voltage monitor channel. Each photometer (PH7 and PH8) required one signal channel and a shared high-voltage monitor channel. Monitors were flown for the boom door ejection (2) and boom deployment (2).

2.3 Multi-Channel Warm Infrared Radiometer (WIRR)

This instrument is a 2-channel filter photometer device using selected InGaAs detectors. The channels will be a 1270 nm O_2 IR atmospheric (0,0) band channel, and a 1350 nm OH Meinel (3,1) band channel. This two channel, chopped device was successfully flown three times onboard the University of Wuppertal Skylark vehicle during the DYANA campaign, and an improved version has successfully flown in the NLC-91 & 93 campaigns onboard a Stockholm University Nike-Orion payload and most recently on CADO-NLC.

3.0 Eddy Rocket Ionization Results

3.1 Electron Density and Structure Measurement

The ionosphere/mesosphere conditions prior to launch were monitored by the nearby Arecibo incoherent scatter radar and a sodium lidar. Figure 2 shows the radar electron density measurements in the altitude range 80 to 110 km from 2000 hours on February 24 to 0800 hours on 25 February. Preliminary analysis by Arecibo scientists indicated a broad peak electron density in the 100 to 105 km region of about 2×10^4 electrons/cm^3 at the time of the Eddy rocket

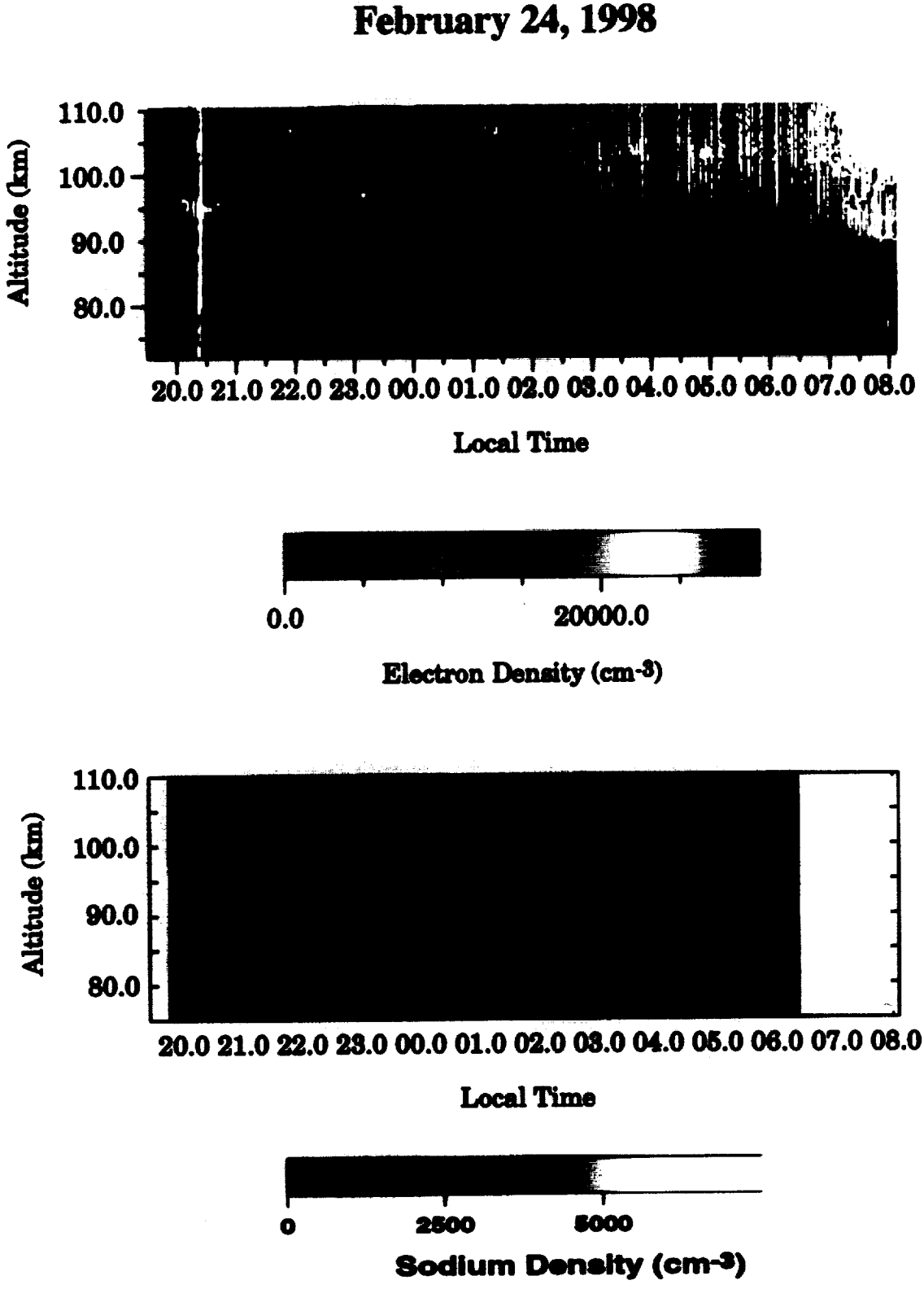

Figure 2 Arecibo radar and lidar measurements – 24 and 25 February 1998

launch. The sodium lidar measurements showed a layer formed before midnight that was well defined at an altitude of 93 km at the Eddy rocket launch.

The Eddy rocket was launched at 0350 LT and reach a peak altitude of approximately 125 km about 3 minutes after launch. The dc probe, for the measurement of electron density and small scale structure, functioned perfectly throughout the entire flight. The dc probe consists of two orthogonal booms with a 1-inch diameter ball that were mounted at the front of the payload, at the separation plane of the nose cone. We had one single channel for the dc probe so we transmit the sum of both booms. When one of the booms was in the velocity vector, the other was in the rocket wake. This would occur twice per rocket spin, which was at 6.25 Hertz. Figure 3 shows, as an example of the data, the rocket ascent data of counts as a function of time – the basic data transmission. There are clearly several layers but note the very small scale, thin layers that are present particularly at the peak of the counts near 104 to 109 seconds. Figure 4 shows this region in more detail in the 100 to 115 second regions. The four layers at the peak are very well defined with widths ranging from about 0.5 to 1.0 seconds. Rocket spin effects are very obvious but note that the envelope of the largest wake effects mimic the envelope of the peak values. If we examine two seconds of the data around 105 seconds (Figure 5), we see the spin effects in more detail. The period is about 12.5 Hertz which is twice the rocket spin frequency.

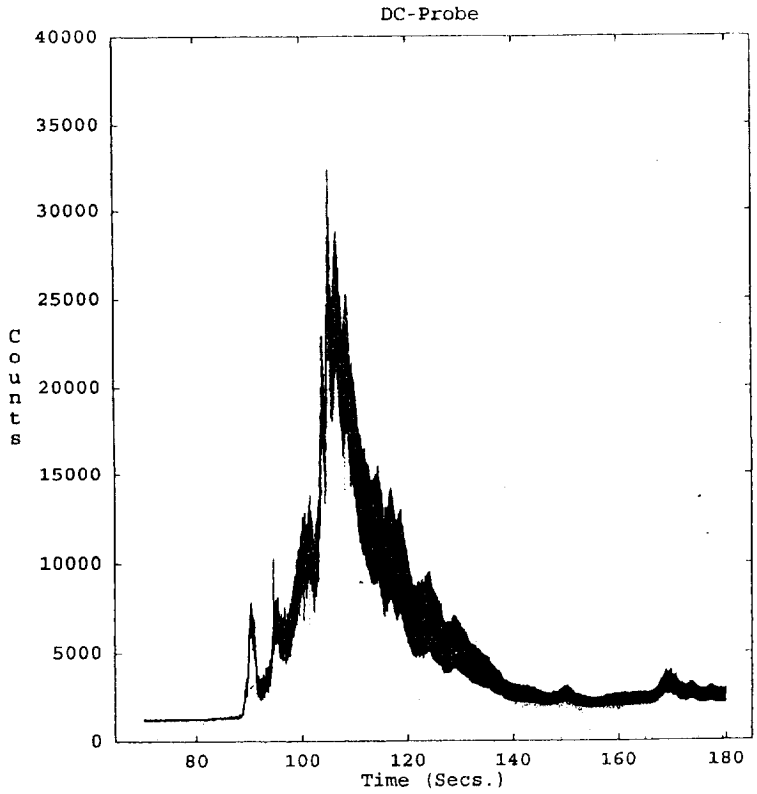

Figure 3 The dc probe measurements on rocket ascent

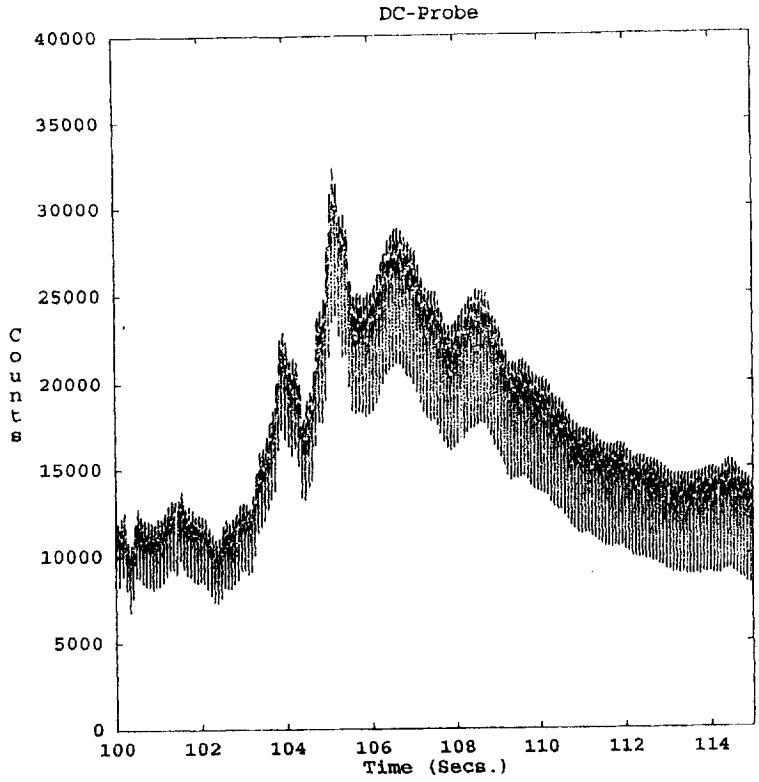

Figure 4 The dc probe measurements at the peak of the E region ionization

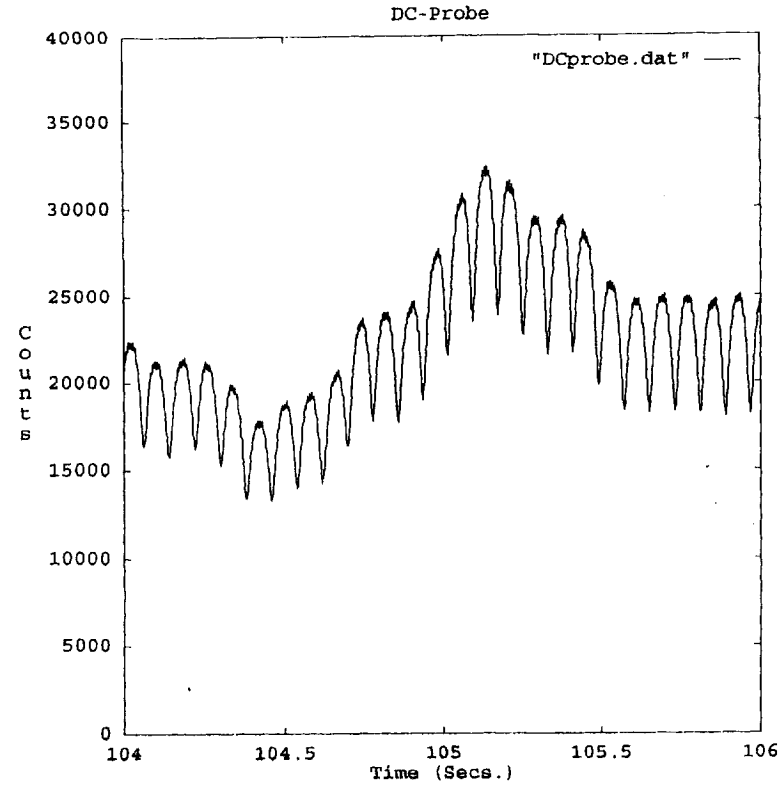

Figure 5 The dc probe data for two seconds showing rocket spin effects

The dc probe counts were converted to currents and these in turn were converted to electron densities using a capacitance probe calibration. Figure 6 shows the rocket ascent and descent electron densities as a function of rocket altitude. The electron density scale at the bottom of the figure corresponds to the rocket ascent results and the rocket descent results are shifted by an order of magnitude. It is obvious that, in general, there is good agreement, particularly with respect to the location at the two layers at about 90 and 94 km and the peak electron density near 103 km, but in fine structure, there are pronounced differences. In general, the ascent results show more fine structure than the descent results above about 100 km. However, if we examine the layer at 90 km, which we presume to be a sporadic E layer, we see three distinct peaks in the descent layer not visible in the ascent results. Note that the electron density peak was approximately 2.0 x 10^4 electrons/cm^3 at about 103 km in agreement with the Arecibo radar results. The layer at approximately 94 km on rocket ascent might be correlated with the sodium layer measured at 93 km. Such a correlation has been suggested by Heinselman, et al., 1998 using higher resolution radar and lidar measurements at Sondrestrom, Greenland.

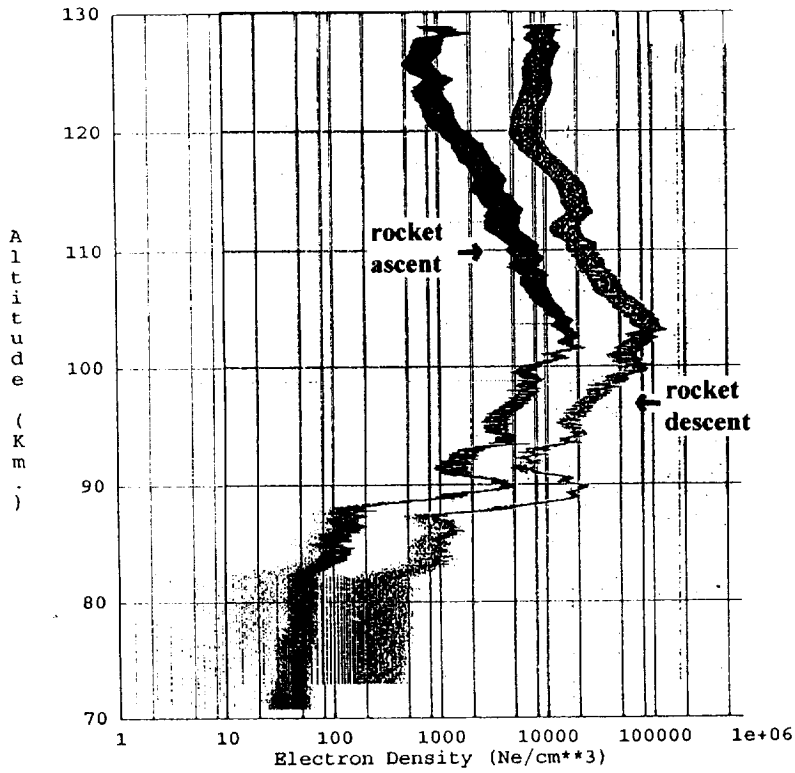

Figure 6 Rocket ascent and descent electron densities as a funciton of altitude; The descent densities are shifted by one order of magnitude

Zhou, et al., 1999, using Arecibo incoherent scatter data to study meteoric impact on the nocturnal E-region electron/ion content, showed a highly structured E-region at six local times (their Figure 4) similar to our Eddy rocket measurements. Further, Yamamoto, et al., 1998 showed electron density profiles of sporatic-E structures from rocket probe measurements during the SEEK campaign at Kyusher Japan that were characterized by highly concentrated thin layers. The formation of such a thin layer was confirmed by comparison with TMA measurements. Larsen, 2000, reported large wind shears that were observed by the Clemson TMA rocket launched 7 minutes before the Eddy rocket. We plan on continuing our investigations using these correlative measurements.

3.2 Mesospheric Turbulence

The agreement and disagreement of our derived energy spectra with the classical model of turbulent theory is critical to our investigation of mesospheric structuring and scattering mechanisms. In turbulent theory the energy spectrum of atmospheric turbulence is divided into several subranges each with its own characteristics. Homogeneous, isotropic turbulence exists in a region called the inertial-convective subrange and is characterized by a spectral slope of –5/3 (see Figure 7). The subrange is bounded by the buoyancy subrange at an "outer scale" L which is determined by buoyancy forces with a spectral slope of –3 and by the viscous-diffusive subrange, with an "inner scale" (Kolmogorov microscale) determined by viscous damping, and with a spectral slope of –7. This classical spectral form has been observed at low latitude using a passive tracer (electron density) as representative of the neutral kinematics (Royrvik and Smith, 1984). However, in the polar summer mesosphere, the ion chemistry is influenced by the cold temperature (lowest in the atmosphere) to such a degree that the energy cascade of the ionized tracer is significantly different from that of the neutral gas flow and creates a new subrange, i.e., the viscous-convective subrange, exhibiting a –1.0 slope transitioning to a –7.0 slope at the "Batchelor scale."Utah State University has been at the forefront of polar mesospheric studies in the last decade, developing and flying probes for the study of the turbulent structure in this fascinating region (e.g. Ulwick et al., 1988; Inhester et al., 1990; and Ulwick et al., 1993). For this investigation we use the same probing techniques to measure the spectra of spatial fluctuations of electron density in order to derive geophysical relevant turbulent parameters such as the heating rate of dissipation of turbulent energy ε and the eddy diffusion coefficient K.

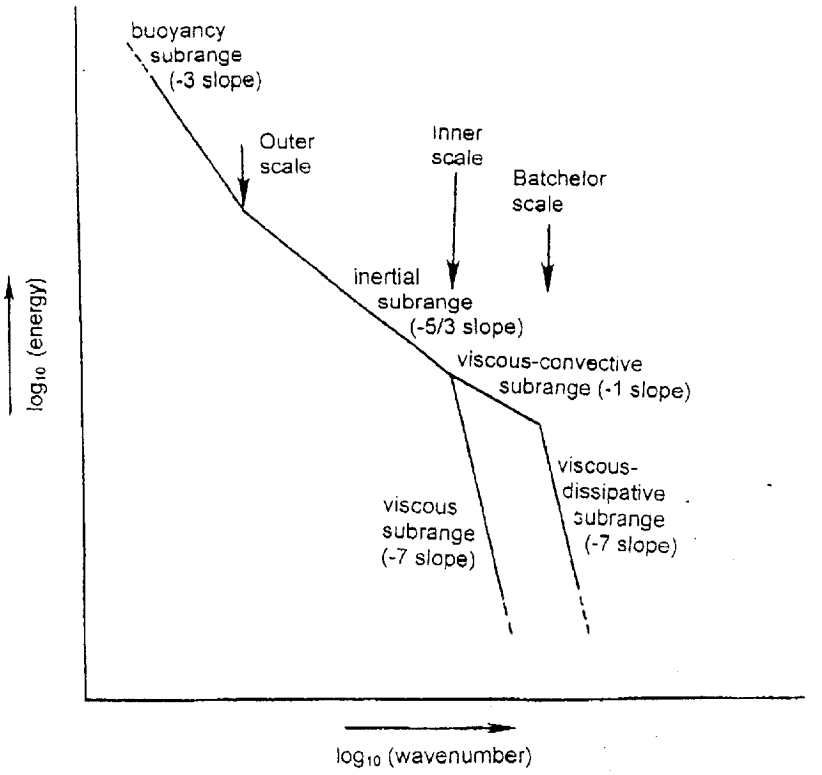

Figure 7 Classical model of turbulent theory but also including the very viscous-convective subrange seen during PMSE

In contrast to the summer polar mesosphere studies where the inner scale of turbulence is difficult to define, the electron density measurement for this campaign conducted at N18° 24′, W66° 26′ should be a true passive tracer of the neutral kinematics. We will use a method after Lubken, 1992, that fits a spectral model to the experimental spectrum which comprises both the inertial-convective and transition to the viscous-diffusive subrange. The model of Tatarskii, 1971, is used and shows the model only depends on two parameters $\tilde{\varepsilon}$ (normalized energy dissipation rate) and N_n (the rate at which the fluctuations of the tracer n are created and at which they disappear). $\tilde{\varepsilon}$ determines the frequency at which the spectrum "breaks" and the combination $N_n \bullet \tilde{\varepsilon}$ ¾ determines the absolute value of the power densities in the intertial-convective range. The theoretical spectrum from Tatarskii, 1971, is fitted to the measured spectrum with standard multi-variate function minimization methods to obtain the best fit values for $\tilde{\varepsilon}$ and N_n. Turbulent parameters are calculated from these parameters such as:

The energy dissipation rate $\varepsilon = (0.033 \bullet a_2)^3 \bullet \tilde{\varepsilon}$ where a is a constant

The structure function constant $$Cn^2 = \frac{N_2}{0.033 \bullet \tilde{\varepsilon}\, 2/3}$$

The eddy diffusion coefficient $K = 0.8 \frac{\tilde{\varepsilon}}{\omega_B}$ where ω_B is the Brunt-Väisälä frequency and

The turbulent velocity $\omega_{Turb} = \sqrt{\frac{\tilde{\varepsilon}}{0.49 \bullet \omega_B}}$ (Weinstock, 1981)

3.3 Turbulent Parameters from Electron Densities

Considering the electron density measurements to be a conservative, passive tracer of neutral density turbulence (Thrane and Grandal, 1981), we derive turbulent parameters from the measurements by spectral analysis using the method described in the previous section. The power spectral analysis of the probe data was performed following the method of Blackman and Tukey, 1958. Spatial power spectra of the relative electron density fluctuations were calculated for 2048 data points in two second intervals from 84 to 106 seconds. Figure 8a shows the rocket data used to obtain power spectra from about 88 seconds to 97 seconds. The data were converted to electron densities for the spectral analysis. The severe contamination of the data due to rocket spin will appear as power spikes at the spin frequency in the spectra. The spectrums before 88 seconds (approximately 88 km) and above 98 seconds (approximately 98 km) were dominated by noise. The five spectrums in the 88 to 98 second interval were very much alike. Figure 8b is the spectrum for the interval from 88 seconds (88 km) to 90 seconds (89.6 km). This spectrum should represent spatial turbulent structure since the time for the rocket to cross them is considerably smaller than the lifetime of turbulent eddies. If the turbulence is stationary, homogeneous, and isotropic, a spectral index of –5/3 is observed for the inertial subrange and a spectral index of –7 for the viscous subrange where the power spectral density falls off steeply. Spectral indices of –7 and –3 are shown but not the index –5/3 for the inertial-convective subrange. The peaks at approximately 6 and 12 Hertz clearly dominate the inertial convective subrange but from power spectral analysis of the measured electron densities, turbulent

parameters are derived. Figure 9a shows the rocket descent data that we used from 267 to 277 seconds, converted to electron densities, for the spectral analysis. We also analyzed the data for rocket descent over the same height interval as we did for rocket ascent. From power spectral analysis of the measured electron densities, turbulent parameters are derived on page 10, Figure 9a shows the spectral index of –7.0 for the viscous subrange and –3.0 for the buoyancy subrange fit the data well. Figure 9b shows the spectrum obtained from the measurements from 273 to 275 seconds (87.3 to 89.1 km). Five spectrums were also obtained in the interval 267 to 277 seconds and they were all the same as Figure 9b. The spectra all were dominated by white noise indicating no turbulent structure. The spin peaks at approximately 6, 12 and 24 Hertz are prominent above the noise.

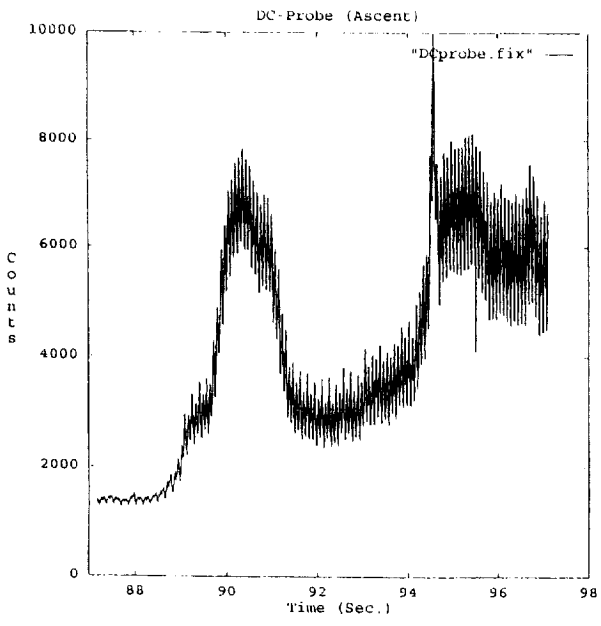

Figure 8a Data on rocket ascent from 88 to to 98 km used in spectral analysis

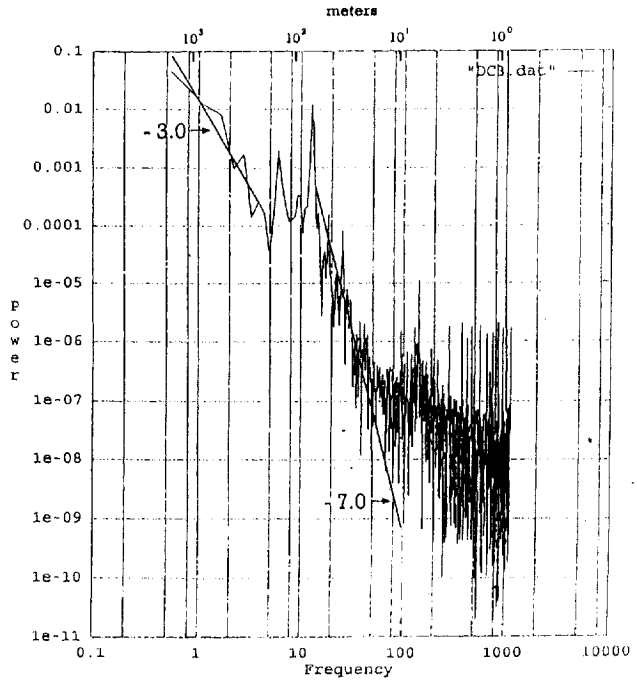

Figure 8b Spectrum from spectral analysis of electron densities from 88 to 90 seconds (88 to 90 km)

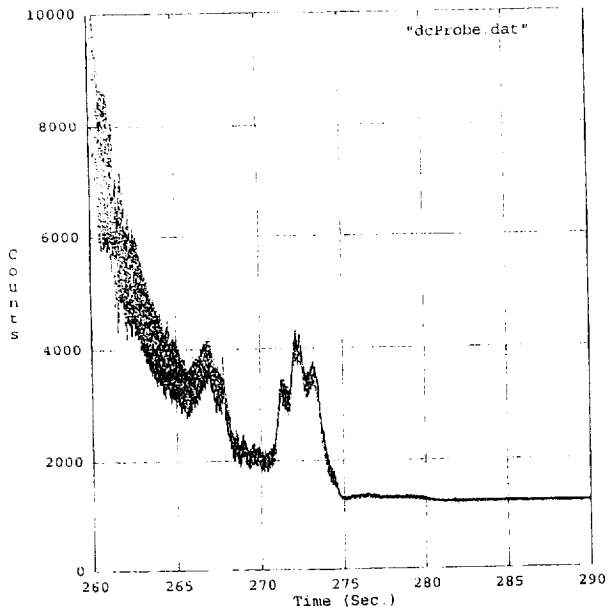

Figure 9a Data on rocket descent used in spectral analysis (265-275 sec)

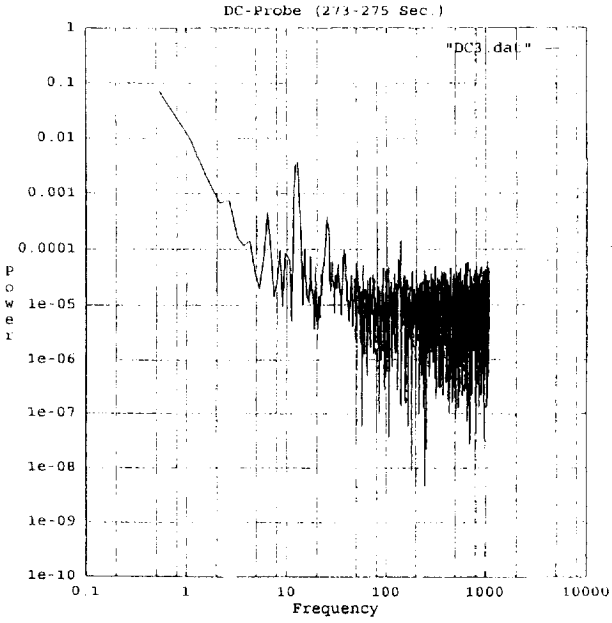

Figure 9b Spectrum from spectral analysis on descent electron densities from 273 to 295

We follow the method previously described to find the model that best fits the data and we superimpose the model onto Figure 10. The model shows the –5/3 spectral index of the inertial convective subrange and viscous damping effects leading to –7.0 spectral index in the viscous subrange. The model gave us an energy dissipation rate (ε) of .044W/kg. We calculated the energy diffusion coefficient, the inner scale and the outer scale using the formulas as previously described. The values are shown beside the spectrum and the inner and outer scale are shown in the figure. The inner scale where the –7.0 slope begins and the outer scale determined by buoyancy forces with a spectral slope of –3.0 seem to fit the data well. Even the dominance of the spin peaks in the inertial subrange does not completely mask the data adherence to –5/3 spectral index between the outer and inner scales

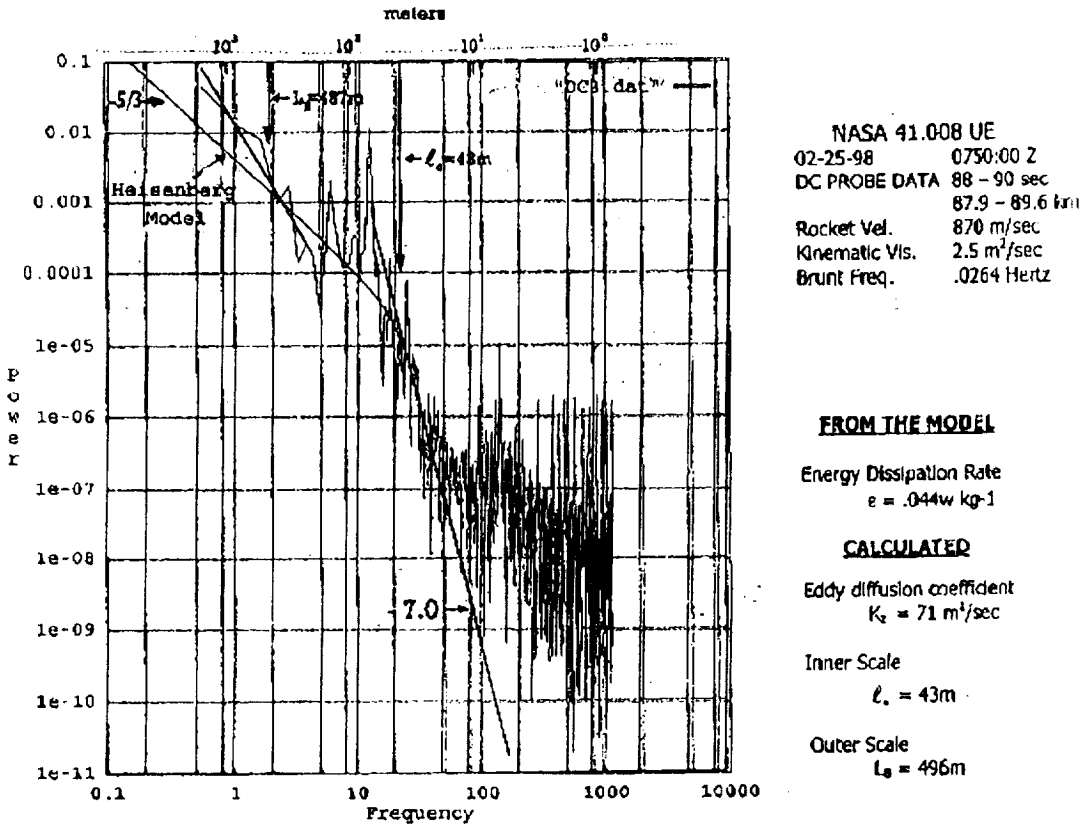

Figure 10 Spectrum from Figure 8 with the Heisenberg model for the E that produced the best fit to the data; Turbulent parameters shown were calculated using this E.

We compare these results with two other rocket measurements of mesospheric turbulence in the equatorial region. In a paper by Goldberg et al., 1997, about a campaign called MATLED conducted at the Alcantara rocket site in northeast Brazil, a power spectrum obtained at 88 km is presented and a Heisenberg turbulence model is fitted to the data. They obtained an epsilon of .027 W/kg and an inner scale of 48.3 meters about the same altitude. Royrvik and Smith, 1984, conducted a rocket and radar investigation on mesospheric turbulence at Punta Lobos, Peru, in February 1983. A single layer of turbulence was observed by both the experiments. The rocket dc probe observed the layer between 85 and 86.4 km. The rocket data shows that the inner scale of turbulence was about 30 meters. Energy dissipation rate in the layer was calculated to be about 0.050 W/kg, which is also in good agreement with our results.

4.0 Atomic Oxygen, Airglow and Modeling Background

4.1 Atomic Oxygen

Of fundamental importance to virtually all aeronomic processes taking place in the mesosphere and lower thermosphere (MALT) is the atomic oxygen (O) density. It is produced by the photo dissociation of O_2 and controlled by photochemical reactions with other odd oxygen and odd nitrogen constituents and by horizontal and vertical transport processes. Its highly reactive nature has made the measurement of even the relative altitude difficult. However, its central role in the photochemistry of the MALT and its dependence on dynamic transport processes make it vital that its concentration be measured simultaneously and with the same, high spatial-resolution as the airglow measurements.

One of the most comprehensive reviews of the role of atomic oxygen in mesospheric chemistry and its inter-relationship with other nightglow and dayglow emissions is contained in the sequence of papers by Greer et al., 1986, dealing with the Energy Transfer in the Oxygen Nightglow (ETON) campaign. Atomic oxygen plays a critical role in the production and loss mechanisms for hydroxyl, ozone, molecular oxygen and a host of metastable O_2 states. In addition, rocket measurements from USU have shown fine scale structure on the atomic oxygen altitude profile which is not due to vehicle motion (Howlett et al., 1980). This structure has been attributed to the passage of a gravity wave through the MALT. Although ground-based measurements of hydroxyl and OI (557.7) nm emissions have shown similar horizontal wave patterns caused by gravity waves (Taylor et al., 1987), it is not known to what degree the atomic oxygen perturbations might drive the other minor species constituents through chemistry.

4.2 OH Airglow

At night, the hydroxyl radical (OH) is produced naturally in the atmosphere in a relatively thin, ~8 km thick layer, at an altitude of ~87 km (Baker and Stair, 1988). The OH formation chemistry produces a strong, chemi-luminescence of the near-infrared, vibration-rotation bands, which were first identified in the night airglow emission by Meinel (1950). The primary chemical source of these bands in the MALT is the reaction of atomic hydrogen with ozone (Bates and Nicolet, 1950). Thus, the strength of these Meinel bands, which radiate most intensely in the spectral region between 1300 and 2400 nm, is related to the mesospheric distribution of water vapor and ozone. These quantities are, in turn, related to the concentrations of atomic and molecular oxygen in the MALT.

Due to the high collision frequency in the MALT, the Meinel band radiation is also quenched by atomic oxygen and hydrogen, as well as by N_2 and O_2 (e.g. Lopez-Moreno et al., 1987). This quenching is also a strong function of the vibrational level of the hydroxyl. Thus, the source distribution, radiative cascade and the quenching reactions all combine in a complex and non-linear fashion to control the distribution of radiance within the vibrational manifold. It is clear from this that these bands are at the center of the odd-oxygen photo-chemistry occurring in the MALT, and that perturbations in the odd-oxygen species will be reflected, or perhaps amplified, in the hydroxyl altitude distribution.

4.3 Modeling

Photochemical-Dynamical models are one of the basic important tools in theoretical studies that are used to simulate and quantitatively predict the global distribution of important and chemically active constituents. Each specie in the atmosphere has its own sources and sinks, in addition to being transported globally by global scale circulation or by various dynamical processes that act on all spatial and temporal scales, such processes include wave breaking and turbulent mixing. Thus, it is critical that these models correctly include quantitative parametrization of transport.

5.0 Hydroxyl Emissions and Atomic Oxygen

We used a warm (non-cryogenic) Infrared Radiometer to measure at 1350 nm the OH Meinel (3, 1) band emission profile. Figure 11 shows the ascent and descent measured radiance from 70 to 120 km. Note the increase in counts above about 90 km which was very strong on rocket ascent.

This glow has been measured in other rocket flights (Lopez-Moreno, et al., 1985; Ratkowski and Ulwick, 1993) which were all in the region above about 92 km and at different OH Meinel bands. Also, on those rocket flights no contamination was detectable at 1.27 μm. This is also true for the 1.27 μm measurements here from the Eddy flight. Murtagh, using a mechanistic analysis, showed that the glow (private correspondence) they measured can be successfully modeled by I proportioned to $[O]^2 V^2$ where V is the rocket velocity.

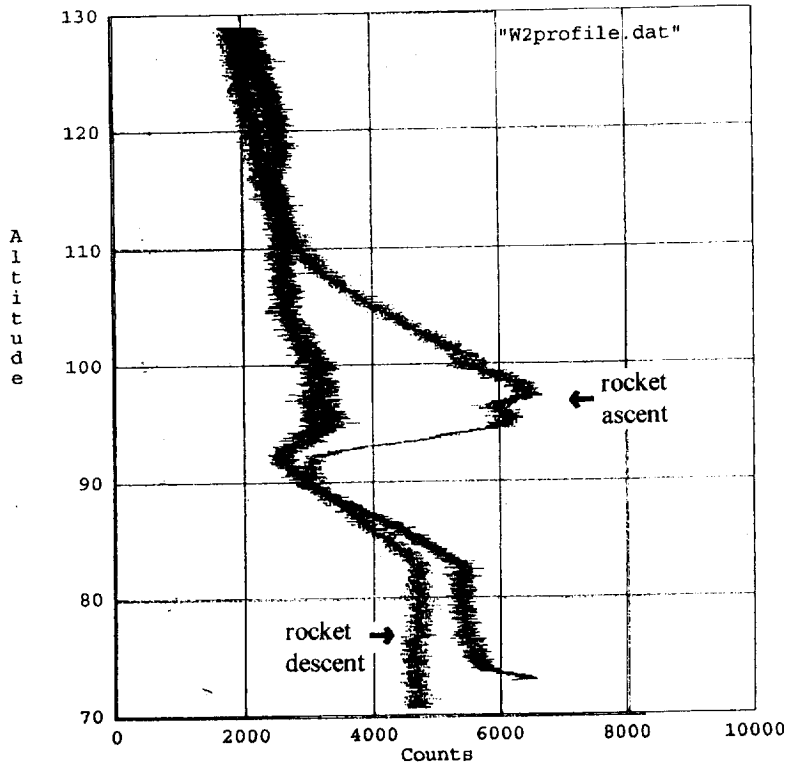

Figure 11 IR radiometric 1350 nm OH Meinel band emission profiles for rocket ascent and descent

Following this method and using the rocket ascent profile above 90 km (Figure 11), we obtained the profile proportional to atomic oxygen shown in Figure 12. From the glow measurements and atomic oxygen measurements (Ratkowski and Ulwick, 1993), we calculated a proportionality coefficient at the peak radiance $k = 6.35 \times 10^8$. We applied this to the Eddy data at 98 km and calculated the atomic oxygen to be approximately 3.0×10^{11} atoms/cm^3.

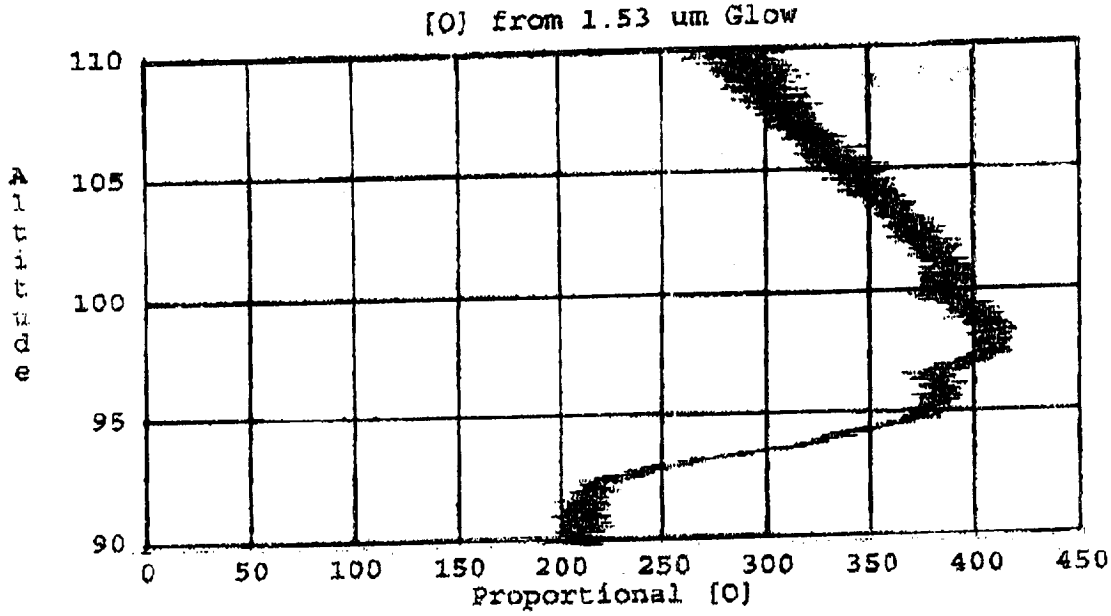

Figure 12 Profile proportional to atomic oxygen from rocket glow measurements using mechanistic analysis

For the Eddy rocket ATOX experiments on booms No. 1 and 2, we were only able to obtain a profile proportioned to the atomic oxygen concentration from the absorption measurements on boom No. 2. There was damage to the detectors on boom No. 1 and the resonance fluorescence experiments failed on both systems. We, therefore, compare relative measurements of atomic oxygen from the absorption measurements for rocket ascent to the profile obtained from the mechanistic analysis of the rocket glow measurements above 90 km. Figure 13 shows the two results. There is good agreement in the profiles particularly with respect to the increase in atomic oxygen above 92 km, the double peaks at 95 and 98 km, and the decreasing values above 98 km or about 105 km.

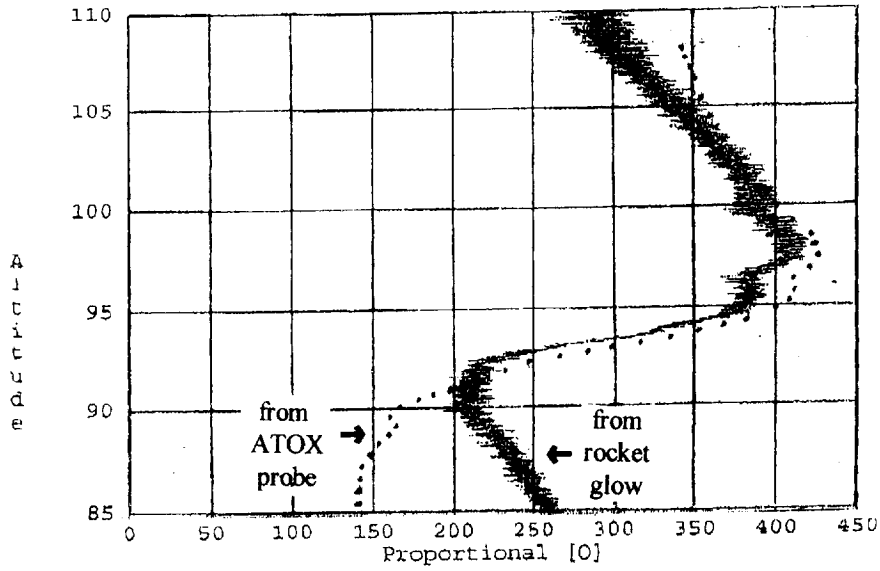

Figure 13 Atomic oxygen profile from absorption measurement compared to glow atomic oxygen profile

5.1 Modeling

We have a 1-D chemical kinetic transport model where the vertical flux of trace constituents is parameterized by an eddy diffusion coefficient (K_{22}). This parametrization has been found to capture the essence of the behavior of long lived species, such as the atomic oxygen distribution in the lower thermosphere and mesosphere. This 1-D model has been used successfully to extract eddy diffusion coefficients using measured atomic oxygen profiles on board rocket experiments during DYANA and MAPWINE campaigns (see Ratkowski et al., 1991; Ratkowski, et al., 1994; Ulwick, et al., 1994). Here we use the eddy diffusion coefficients obtained from the electron density power spectral analysis to obtain an atomic oxygen profile and an OH radiance profile to compare with the measurements. We superimpose the modeling results on the measurement shown in Figure 13 for atomic oxygen and the OH radiation descent profile shown in Figure 12. In both cases we had to shift the modeling results upward in altitude to obtain the best fit to the measured profiles as shown in Figures 14 and 15.

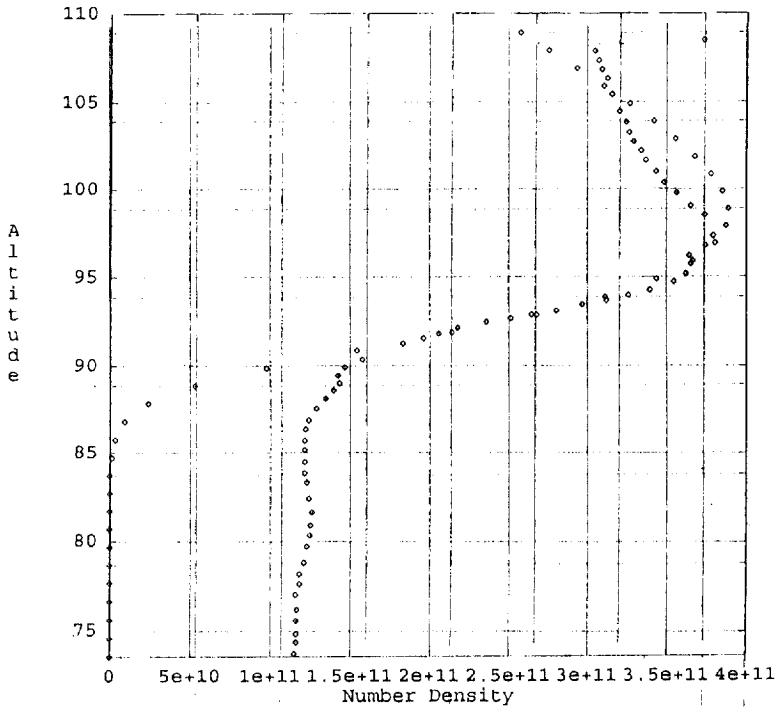

Figure 14 Atomic oxygen profile from modeling compared to absorption measurement profile

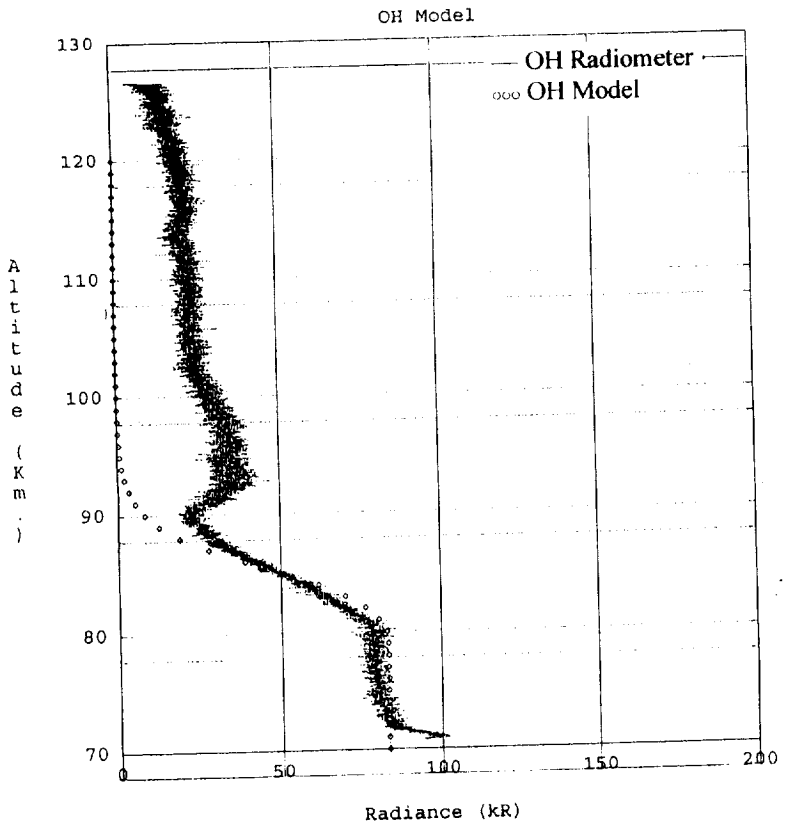

Figure 15 Rocket measurements on descent of OH radiance compared to model calculations

6.0 Summary

The abstract pretty well summarizes the results of this investigation to date. The early results were presented at the Coqui Dos session at the 1998 Fall AGU Meeting in San Francisco, CA. We will continue our data analysis, especially on the discrepancy between the rocket results and our modeling results or both OH radiance and atomic oxygen profiles. We feel that the electron density results could be pursued further with respect to the observed structures. Correlation with wind shear measurements and turbulence and a paper for publication could result. Three people at the Stewart Radiance Laboratory of the Utah State University Research Foundation were involved in the data processing and analysis. James C. Ulwick is the Principal Investigator, Charles Eastman processed all the data and Usama Mahklouf was responsible for the modeling work.

REFERENCES

Baker, D.J. and A.T. Stair, Jr., Rocket measurements of the altitude distributions of the hydroxyl airglow, *Physica Scripta*, 37, 611, 1988.

Bates, D.R., and M. Nicolet, The photochemistry of atmospheric water vapor, *J. Geophys. Res.*, 55, 301, 1950.

Goldberg, R.A., G.A. Lehmacher, F.J. Schmidlin, D.C. Fritts, J.D. Mitchell, C.L. Croskey, M. Friedrich, and W.E. Swartz, "Equatorial Dynamics Observed by Rocket, Radar, and Satellite During the CADRE/MALTED Campaign: 1. Programmatics and Small Scale Fluctuations," *J. Geophys. Res., 102,* 26179-26190, 1997

Greer, R.G.H., D.P. Murtagh, I.C. McDade, P.H.G. Dickinson, L. Thomas, D.B. Jenkins, J. Stegman, E.J. Llewellyn, G. Witt, D.J. Mackinnon and E.R. Willians, ETON 1: a data base pertinent to the study of energy transfer in the oxygen nightglow, *Planet Space Sci.*, 34, 771, 1986.

Heinselman, C.J., J.P. Thayer, and B.J. Watkins, A high-latitude observation of sporadic sodium and sporadic E-layer formation, *Geophys. Res Let.*, 25, 16, 3059-3062, 1998.

Howlett, L.C., K.D. Baker, L.R. Megill, A.W. Shaw, W.R. Pendleton and J.C. Ulwick, Measurement of a structured profile of atomic oxygen in the mesosphere and lower thermosphere, *J. Geophys. Res.*, 85, 1291, 1980.

Inhester, B., J.C. Ulwick, J. Cho, M.C. Kelley, and G. Schmidt, Consistency of rocket and radar electron density observations: implications about the anistropy of mesospheric turbulence, *J. Atmos. Terr. Phys.*, 1990.

Larsen, M.F., Coqui EI mesospheric and lower thermosphere wind observations over Puerto Rico, *Geophys. Res. Let.*, 27, 4, 2000.

Lopez-Moreno J.J., R. Rodrigo, F. Moreno, M. Lopez-Puertas and A. Molina, Altitude distribution of vibrationally excited states of atmospheric hydroxyl at levels v=2 to v=7, *Planet Space Sci.*, 35, 1092, 1987.

Lubken, F.J., On the extraction of turbulent parameters from atmospheric density fluctuations, *J. Geophys. Res.*, 97, 20385, 1992.

Makhlouf, U., R.H. Picard, and J.R. Winick, Photochemical-dynamical modeling of the measured response of airglow to gravity waves, submitted to *J. Geophys. Res.*, 1994.

Meinel, A.B., OH emission bands in the spectrum of the night sky, *I. Astrophysical J.*, 111, 555, 1950.

Ratkowski, A.J., J. Ulwick, Twilight measurements of high-latitude atmospheric minor species during the DYANA campaign, *Proc. Tenth European Space Agency Symposium on European Rocket and Balloon Programmes* and related research, Mandelieu-Cannes, France, 1991.

Ratkowski, A. J., R.H. Picard, J.R. Winick, U.B. Makhlouf, J.C. Ulwick, K.U. Grossmann, D. Homann, J. Schultz, and A.J. Paboojian, Rocketborne measurements and modeling of summer high latitude nitric oxide, *Proc. 11th European Space Agency Symposium*, Montreux, Switzerland, 1994.

Ratkowski, A.J., and J.C. Ulwick, Rocket measurements of high-latitude summer mesosphere [O], OH^2, $O_2(^1\Delta_g)$ and spacecraft airglow, in
airglow and aurora, Sergej Leontiev, Editor, *Proc. SPIE 2050*, 1993.

Royrvik, O. and L.G. Smith, Comparison of Mesospheric VHF Radar Echoes and Rocket Probe Electron Concentration Measurements, *J. Geophys. Res.*, 89, A10, 9014-9022, 1984.

Tatarskii, V.I., The effects of the turbulent atmosphere on wave propagation, *Israel Program for Scientific Translations*, Jerusalem, 1971.

Taylor, M.J., M.A. Hapgood, and P. Rothwell, Observations of gravity wave propagation in the OI (557.7 nm), Na (589.2 nm) and the near infrared OH nightglow emissions, *Planet. Space Sci.*, 35, 413, 1987.

Thrane, E.V. and B. Grandal, Observations of fine scale structure in the mesosphere and lower thermosphere, *J. Atmos. Terr. Phys.*, 43, 179-189, 1980.

Ulwick, J.C., K.D. Baker, M.C. Kelley, B.B. Balsley, and W.L. Ecklund, Comparison of simultaneous MST radar and electron density probe measurements during STATE, *J. Geophys. Res.*, 93, 1988.

Ulwick, J.C., A.J. Ratkowski, and U.B. Makhlouf, "Twilight rocket measurements of high-latitude atomic oxygen density during the DYANA campaign, *J. Atmos. Terr. Phys.*, in press, 1994.

Ulwick, J.C., M.C. Kelley, C. Alcala, T.A. Blix, and E.R. Thrane, Evidence for two different structuring and scattering mechanisms and the associated role of aerosols in the polar summer mesosphere, *Geophys. Res. Let.*, 20, 20, 2307, 1993.

Yamamoto, M., T. Ono, H. Oya, R.T. Tsunoda, M.F. Larsen, S. Fukao, and M. Yamamoto, Structures in sporadic-E observed with an impedance probe during the SEEK campaign: comparisons with neutral-wind and radar-echo observations, *Geophys. Res. Let.*, 25, 11, 1781-1784, 1998.

Zhou, Q. H., J.D. Mathews, and Q.N. Zhou, Incoherent scatter radar study of the impact of the meteoric influx on nocturnal E-region ionization, *Geophys. Res. Let.*, 26, 13, 1833-1836, 1999.